Particle in a variable-size box: The influence of the tip in thin-film electron interferometry

J. A. Kubby and W. J. Greene
Xerox Webster Research Center, 800 Phillips Road, Webster, New York 14580
(Received 20 May 1993)

The influence of the scanning-tunneling-microscopy tip on the conductance spectra measured in thin-film electron interferometry is considered, and is discussed in terms of coupled quantum wells. One of the wells is formed by the linear potential drop between the tip and sample, which gives rise to vacuum-field-emission resonances. The spectra of field-emission resonances are shown to be very sensitive to the properties of the tip, and can be understood in terms of confining the electron to triangular potential wells of different sizes. The other potential well is formed within the thin-film adlayer, and its spectrum should be largely independent of the properties of the tip. We consider the spectrum of the coupled system, and discuss it in terms of perturbation theory where we observe the tendency of the levels to repel each other when they are closely spaced in energy, and to cause level splitting when the levels are degenerate.

I. INTRODUCTION

The vacuum gap between the tip and sample in a scanning tunneling microscope (STM) provides near ideal conditions for the realization of a particle in a triangular potential well. When the applied gap bias in the tunneling microscope exceeds the image-reduced barrier height of the sample, the tunneling electron can have a positive kinetic energy within the gap, leading to the formation of electron standing waves at biases close to the bound states of an electron in a triangular potential well.[1–5] The standing waves result from constructive interference between incident and reflected electrons in the positive kinetic-energy region of the vacuum gap, between the classical turning point marked Z_T and the sample surface at $Z=0$ in the potential energy diagram shown in Fig. 1. The first two standing-wave states have been labeled as $m=1,2$ in the figure. In addition to these vacuum-field-emission resonances, we have found that additional resonances can be excited within thin-film overlayers, one of which has been labeled $n=1$ in the figure. This standing wave has been formed within the overlayer from constructive interference between reflections from the δ function V_S at the surface of the sample, $Z=0$, and the δ function V_i at the films interface to the substrate at $Z=Z_0$. These δ functions have been chosen to characterize the thin-film overlayer as they are the simplest way to model the rapid variation in potential that occurs at the vacuum-overlayer and overlayer-substrate interfaces. The solution of Schrödinger's equation for this model potential has been described by Wang, Kubby, and Greene.[6] In a previous publication we have shown that these thin-film resonances occur in spectra collected over certain geometric arrangements of tin on a silicon surface and are absent over other arrangements, and have compared spectra collected over each of these areas for a single tip.[7] In the following we compare spectra collected with different tunneling tips over equivalent regions of the sample that support the formation of thin-film standing-wave resonances. As the STM tip can be the weak point of tunneling spectroscopy, with atomic scale properties that are for the most part not under experimental control, it is important to see how these properties, which can vary daily, effect the measured thin-film electron standing-wave spectra.

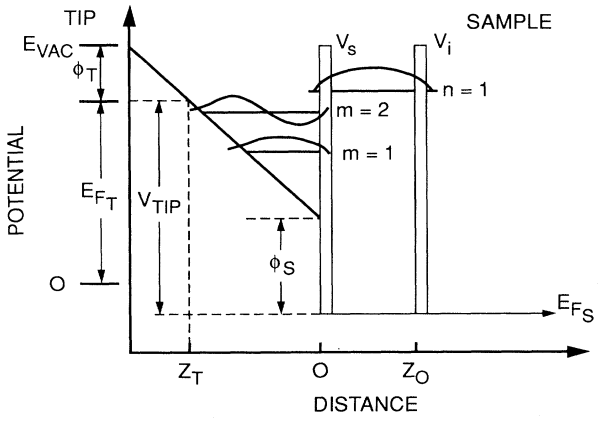

FIG. 1. Potential-energy diagram between the tip and sample. The Fermi level of the tip, E_{FT}, is displaced from the Fermi level of the sample, E_{FS}, by the applied bias V_{tip}. The work function of the tip and sample are ϕ_T and ϕ_S, respectively. The electron has a positive kinetic energy in the triangular potential well formed between the classical turning point, Z_T, and the sample surface at $Z=0$, when $V_{tip}>\phi_S$. Under these conditions, standing-wave states form within the well, and have been labeled as $m=1$ and 2. The overlayer, of thickness Z_0, has been modeled by δ-function scattering potentials at the surface, V_S, and at the interface to the substrate by V_i. A standing-wave state within the overlayer has been labeled $n=1$.

II. A PARTICLE IN A VARIABLE-SIZE BOX

In thin-film electron interferometry, a slow bias ramp is applied to the STM probe tip, which causes it to retract

from the sample surface under feedback control, so as to maintain a constant demanded tunneling current.[1,2] A small high-frequency dither voltage, beyond the bandwidth of the feedback loop, is added to the tip bias to perform modulation spectroscopy. In this way it is possible to record the gap conductance spectra dI/dV as a function of the ramp bias voltage V, by recording the output of a lock-in amplifier that detects the in-phase component of the tunnel current.[2] The trajectory taken by the tip is also recorded by monitoring the feedback correction voltage, yielding the tip's displacement away from the surface as a function of bias. The trajectory taken by the tip, $S(V)$, will depend upon the relationship between the applied bias and the tunnel current: the I-V characteristic for the device. The majority of the structure in standing-wave spectra occurs in the high-negative-bias regime, beyond -5 V tip bias, where dI/dV vs V exhibits oscillations[2] and $S(V)$ exhibits kinks in the tip trajectory,[1] which are associated with the formation of standing waves in the positive kinetic-energy region between the tip and sample. As the tip retracts from the sample, standing waves are excited at biases close to the bound states within the related triangular potential well.[5]

An example of two conductance and trajectory spectra collected over *identical* Sn/Si(111)-$2\sqrt{3}\times 2\sqrt{3}$ surface reconstructions, *but on different days,* are shown in Figs. 2(a) and 2(b). Both spectra exhibit conductance oscillations and kinks in the tip trajectory beginning at around -5 V tip bias; however, the number of conductance oscillations and kinks in the tip trajectory, as well as the total tip displacements, are different between the two spectra. In Fig. 2(a), the tip is displaced by 20.1 Å when the bias voltage is ramped from -1 to -10 V, whereas the tip is displaced by an additional 4.9 Å in the spectrum shown in Fig. 2(b), resulting in a wider potential well. In addition, the conductance goes through five oscillations between -5- and -10-V bias, labeled $m=1-5$ in Fig. 2(a), whereas the conductance goes through six oscillations in the same bias interval, labeled $m=1-6$ in Fig. 2(b). In this way it can be seen that the wider potential well in Fig. 2(b) is able to support an additional standing-wave state relative to the potential well in Fig. 2(a). *As both spectra were collected over identical* $2\sqrt{3}\times 2\sqrt{3}$ *surface reconstructions, the differences between them must be due to differences in the probe tips on the different days.*

The characteristics of the triangular potential well are strongly dependent on the properties of the tip, as can be seen by consideration of the Fowler-Nordheim equation[8] which approximately describes the I-V characteristic for a blunt tip in the high-bias regime[9,10]

$$I(V)=\alpha AF^2(V)\frac{(\mu/\varphi)^{1/2}}{\varphi+\mu}\exp\{-\beta\varphi^{3/2}/F(V)\}\ , \qquad (1)$$

where A is the effective tunneling area, $F(V)$ is the field, and φ and μ are the work function and Fermi energy of the tip, respectively. The most important tip-dependent factors are those within the exponential, although the effective tunneling area will also have a weak influence. The properties of the tip within the exponential are both the tip work function φ, as well as the relationship between the applied voltage and the field, $F(V)$. For a blunt tip, where the radius of curvature r is much greater than the vacuum gap, on the order of 10–30 Å, the field is essentially constant and is given by the ratio of the applied voltage V to the gap distance d, $F=V/d$, as in a parallel plate capacitor. This relationship leads to a triangular potential well, and is considered here for simplicity. The case for a sharp tip is discussed below.

A typical value for a tungsten tip work function would be 4.5 eV, and previous investigations have found that a field of 0.38 V/Å is sufficient to draw a field-emission current on the order of a few nA.[10] In Fig. 3(a) we show a triangular potential well with a slope of 0.38 V/Å, and have drawn in the first five bound states for this potential. The solutions of the Schrödinger equation for an infinite triangular potential well are Airy functions, where the energy eigenvalues are given asymptotically for large n by[11]

$$E_n=(\hbar^2/2m)^{1/3}(3\pi F/2[n+\tfrac{3}{4}])^{2/3},\quad n=0,1,\ldots, \qquad (2)$$

where F is the applied field. The exact eigenvalues have $(n+\frac{3}{4})$ in Eq. (2) replaced by 0.7587, 1.7540, and 2.7575, respectively, for the three lowest solutions. We show the

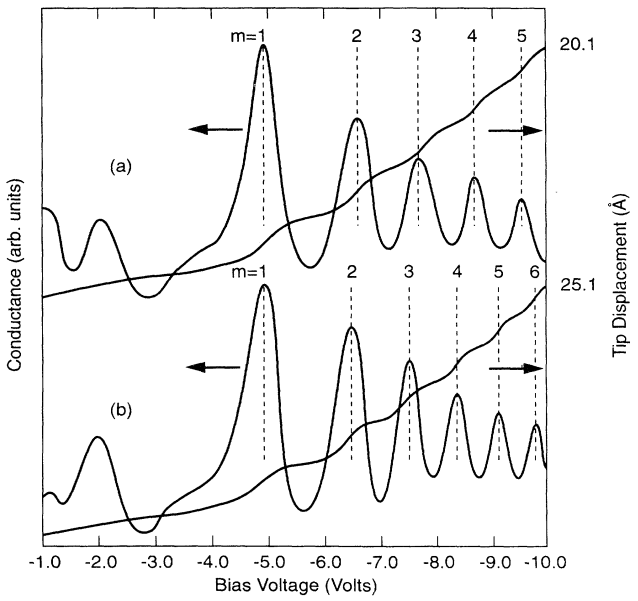

FIG. 2. Electron standing-wave conductance spectra dI/dV (left axis) and tip trajectories $S(V)$ (right axis) as a function of tip bias V, collected over $2\sqrt{3}$ domains of Sn/Si(111). The data in (a) and (b) were collected on different days with the same demanded tunneling current of 1 nA. Variations in the properties of the tip have led to the differences in the conductance spectra. In (a), the tip supported five field-emission barrier resonances between -5 and -10 V which have been labeled as $m=1,\ldots,5$, while in (b) the tip supported six field-emission barrier resonances which have been labeled as $m=1,\ldots,6$. Corresponding differences in the tip trajectories can also be seen; (a) has five kinks between -5 and -10 V bias and has been displaced by 20.1 Å, while (b) has six kinks and has been displaced by 25.1 Å.

bound states up to 7 eV to compare with the thin-film electron standing-wave spectra, which are generally collected up to 10 eV. The ~3-eV difference between the two is the applied bias needed to exceed the image-reduced barrier height of the sample,[12] after which the electron has a positive kinetic energy within the gap. If the tip work function is lowered by adsorption of contaminants, possibly from the transfer of sample material onto the tip, the field required to draw the same amount of field-emission current would be lower by an amount $F_2=(\varphi_2/\varphi_1)^{3/2}F_1$ according to the exponent in Eq. (1). In Fig. 3(b) we have drawn the triangular potential well which would result from lowering the tip work function by 0.5 eV, which lowers the field required to draw the same amount of field-emission current to 0.32 V/Å. It can be seen that the triangular potential well has broadened, resulting in a lowering and closer spacing of the well levels, allowing an extra level to be pulled in from the top. Now there are six bound states within the same well depth of 7 eV. Lowering the tip work function by an additional 0.5 eV results in a required field of 0.26 eV, allowing an additional bound state to exist as shown in Fig. 3(c). In this way it can be seen that variation of the tip work function results in the variation of the size of the triangular potential well and the related variation of the associated bound-state energy eigenvalues. As the well broadens, the energy levels are lowered and they become more closely spaced, allowing new levels to be brought in from above. *Thus the number of bound states within a given energy interval, as well as their position, can vary with the properties of the tip.*[13]

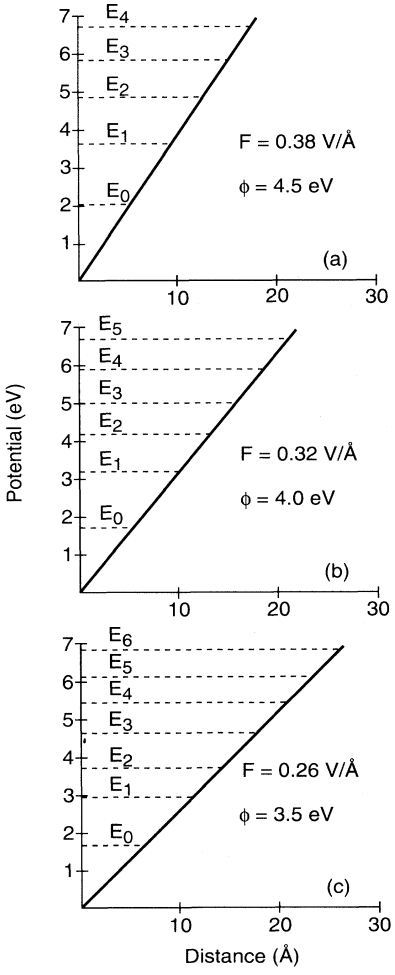

FIG. 3. Solutions to the Schrodinger equation for an infinite triangular potential well of various widths; (a) 18.4 Å wide, $F=0.38$ V/Å; (b) 21.9 Å wide, $F=0.32$ V/Å; and (c) 26.9 Å wide, $F=0.26$ V/Å. The energy eigenvalues have been drawn in and labeled as E_n.

Above we have only considered a change in a blunt tip's work function. The sharpness of the tip is also a variable which can change depending on tip processing, such as drawing heavy field-emission currents for cleaning, field-induced rearrangements of the tip apex, and accidental tip-sample contact. These processes can effect the electrostatic field distribution around the tip's apex, $F(V)$, and consequently the relationship between the applied voltage and the tip-sample distance as determined by Eq. (1). Pitarke, Flores, and Echenique[14] have calculated the tip-sample distances as a function of applied voltage for tips with varying radii of curvature. They found that the $S(V)$ curves were very dependent on the tip radius for curvature less than ~100 Å. *At a given applied bias, a sharp tip obtains a given field further from the surface than a flat tip, and thus the potential well is broader.*

It can be seen from the previous discussion that any change in the work function or sharpness of the tip will lead to large changes in the size of the triangular well potential, as the $S(V)$ characteristic depends exponentially on these tip characteristics through the Fowler-Nordheim equation (1). Since the number of vacuum barrier resonances within a given energy interval as well as their peak positions are variable, the positions of these peaks could have an important influence on thin-film standing-wave spectra, especially if the resonance energies happen to coincide. After briefly reviewing the spectra of thin-film standing-wave states for various areas on the sample as measured by a single tip, we will come back to determine the influence of making these same measurements using different tips.

III. THE INFLUENCE OF THE SAMPLE IN THIN-FILM ELECTRON INTERFEROMETRY

In previous publications we have shown that the detailed structure of electron standing-wave spectra can have a dependence on the area of the surface over which it is collected, particularly for spectra collected over thin-film adlayers, and thus may provide useful information for characterizing these thin films.[7,15,16] Here we briefly review the results for the various heterointerfaces formed between tin and silicon. This system is of interest as it forms an interface that is atomically abrupt and epitaxial, and thus well defined.

Tunneling topographic images are shown in Fig. 4 for the various reconstructions of tin on silicon;[17–19] Fig. 4(a) shows a boundary between a domain of $2\sqrt{3}$ recon-

struction and a domain of $\sqrt{3}$ reconstruction, and Figs. 4(b), 4(c), and 4(d) show a domain of a surface alloy formed between tin and silicon imaged under various biasing conditions, as discussed below. The alloy has been labeled as "$\sqrt{3}$ mosaic" and comprises frustrated atom chains, visible in the filled-state image shown in Fig. 4(b), which are similar to the frustrated atom chains found for surface alloys of lead and silicon.[20] The $2\sqrt{3}$ and $\sqrt{3}$ reconstructions were prepared by deposition of approximately $\frac{1}{3}$ ML (monolayer) of tin onto the room-temperature substrate from a tungsten-filament source at a deposition rate of 1 ML/min. After deposition, the sample was annealed at 550 °C for 2 min to generate the $2\sqrt{3}$ and $\sqrt{3}$ reconstructions, and at 800 °C to generate the $\sqrt{3}$ mosaic surface.

In Fig. 5 we show electron standing-wave spectra collected over each of these different surface reconstructions. In Fig. 5(a) the spectrum was collected over the $2\sqrt{3}$ domain, to the left in Fig. 4(a), with the dominant features being the vacuum barrier resonances that begin at around -5.0-V tip bias, similar to the spectra shown in Fig. 2 which were also collected over $2\sqrt{3}$ domains. If the spectrum is collected over the $\sqrt{3}$ domain, to the right in Fig. 4(a), the resulting spectrum is different as shown in Fig. 5(b). In this spectrum there is a disruption in the vacuum-field-emission resonances at -7.5-V bias, that appears to split the $m=3$ barrier resonance into two peaks. This disruption has been labeled with an arrow in the figure. In addition to splitting the $m=3$ resonance, the higher-order resonances in Fig. 5(b) have been phase

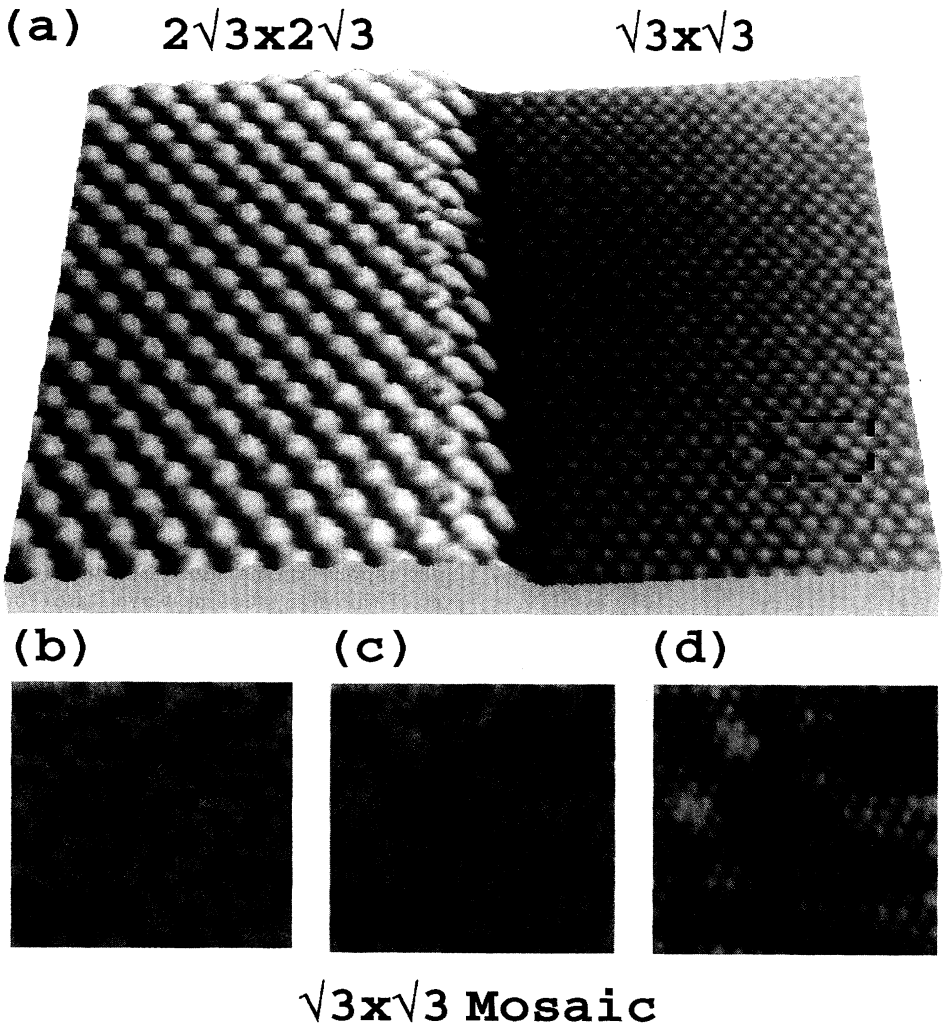

FIG. 4. Tunneling topographs of areas used for electron standing-wave excitation. (a) 250X 250-Å area containing $2\sqrt{3}$ reconstruction on the left and $\sqrt{3}$ reconstruction on the right. Some defects in the $\sqrt{3}$ domain have been outlined with a box. The image was collected at a tip bias of -1.5 V, tunneling into the sample empty states at a demanded tunneling current of 1 nA. (b) 100X100-Å domain of $\sqrt{3}$ mosaic, tunneling out of the samples filled states at a tip bias of $+1.0$ V, 1 nA. The corresponding empty-states image, collected simultaneously at -1.0 V, is shown in (d). The two are overlayed and the composite image is shown in (c).

shifted by 180° from the resonances in Fig. 5(a); beyond −7.5-V bias the peaks in the $2\sqrt{3}$ spectrum line up with the valleys in the $\sqrt{3}$ spectrum. Dashed lines have been drawn in to guide the eye in seeing this phase shift. If the spectrum is collected with the tip centered over one of the defects in the $\sqrt{3}$ domain, that have been labeled with a dashed box in Fig. 4(a), the resulting spectrum shown in Fig. 5(c) no longer has the disruption in the barrier resonances at −7.5-V bias, and the phase shift in the higher-order resonances is much less than 180°. If the spectrum is collected over the $\sqrt{3}$ mosaic domain shown in Fig. 4(b), the resulting spectrum shown in Fig. 5(d) also has no disruption in the barrier resonances at −7.5-V bias, and once again the phase shift of the higher-order resonances is minimal.

We have previously ascribed the disruption at −7.5 V bias in the vacuum-field-emission resonances collected over $\sqrt{3}$ domains to the formation of electron standing-wave resonances that result from the constructive interference between electrons reflected at the vacuum-tin and tin-silicon interfaces.[7] This resonance has been labeled as $n=1$ in the potential-energy diagram shown in Fig. 1. The lack of a standing-wave formation over the $2\sqrt{3}$ domain can be understood from consideration of its different geometric structure. The formation of electron standing waves requires that the overlayer and substrate reflect electrons strongly, and the reflectivity of the overlayer will depend on its geometric structure; the longer surface periodicity of the $2\sqrt{3}$ domain would tend to scatter electrons more strongly relative to the shorter periodicity of the $\sqrt{3}$ domain. At a periodic surface an electron can be scattered by a reciprocal-lattice vector; for a short-period surface such scattering is unimportant as even the smallest nonzero reciprocal-lattice vector is too large to scatter an electron with $k_{\parallel}\approx 0$ to another point on the Fermi surface. For a longer surface periodicity, such scattering becomes more important, and the electron can be diffracted into other beams. In this way it can be seen that the expected strength of standing-wave resonances that result from reflections between periodic interfaces would decrease in going from a $1X1$ bulk-terminated surface, with $a_0=3.8$ Å to a $\sqrt{3}$ surface with a periodicity of 6.6 Å, and even further for a $2\sqrt{3}$ surface with a periodicity of 13.2 Å. This can be compared to the effective de Broglie wavelength of a 7.5-eV electron which would be 4.5 Å.

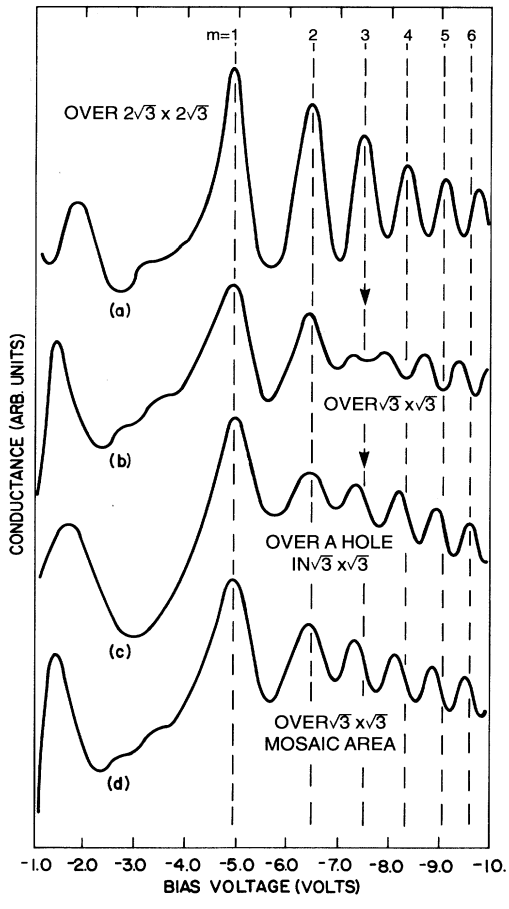

FIG. 5. Electron standing-wave spectra collected over various surface reconstructions; (a) over a $2\sqrt{3}$ domain, (b) over a $\sqrt{3}$ domain, (c) over a defect in a $\sqrt{3}$ domain, and (d) over a $\sqrt{3}$ mosaic domain. These various domains are shown in Fig. 4.

The defects in the $\sqrt{3}$ surface, outlined by the box in Fig. 4(a), create an area on the surface that is capable of scattering electrons into many directions, thus suppressing the formation of standing-wave resonances. This expectation is borne out, as can be seen from the lack of structure at −7.5-V bias in the spectrum shown in Fig. 5(c).

The $\sqrt{3}$ mosaic appears to be similar to the $\sqrt{3}$ domain in the empty-state image shown in Fig. 4(d); however, it has a mosaic appearance in the filled state-image shown in Fig. 4(b). We attribute the appearance of the mosaic to an alloy which is formed through the intermixing of tin and silicon atoms due to the higher-temperature processing used to generate this surface. From the overlay shown in Fig. 4(c) it is clear that the $\sqrt{3}$ surface shown in Fig. 4(d) is in registry with the atom chains that are shown in Fig. 4(b). The simplest explanation for this observation is that only one species of the two populations is visible in the filled-state image, whereas both species are visible in the empty-state image. If differences in scattering from different atomic species are taken into account, this surface is locally as defective as the $\sqrt{3}$ defect region outlined in Fig. 4(a), and thus would be expected to suppress standing-wave formation through defect scattering. Indeed the standing-wave spectrum over this area shown in Fig. 5(d) is similar to the standing-wave spectrum over the $\sqrt{3}$ defect region shown in Fig. 5(c). *While the resonance at −7.5 eV found over the $\sqrt{3}$ domain is missing, the density of states in the region between −1.0 and −5.0 eV is identical between these two spectra.* In this way it can be seen that the density of states at −7.5 eV, that we associate with the geometric structure of the thin film, is distinct from the density of states below −5.0 eV that are usually associated with the chemical bonding of the atomic species.

IV. THE INFLUENCE OF THE TIP IN THIN-FILM ELECTRON INTERFEROMETRY

As described above, the properties of the tip determine the trajectory taken by the tip in the field-emission region, and thus control the number and position of conductance oscillations in the barrier resonances. On the other hand, the thin-film interference effects seen at -7.5 eV when taking standing-wave spectra over the $\sqrt{3}$ domains should not be affected by the properties of the tip if they are truly properties of the thin film. This can be tested by taking spectra over $\sqrt{3}$ domains with tips that support different numbers of barrier resonances. It has been found experimentally that the number of standing waves within the bias interval of -5 to -10 eV varies from day to day; thus comparing data taken on different days allows for collecting data with effectively different tips. Alternatively, as the demanded tunneling current determines the starting point of the electron interferometer, as well as the field necessary to draw the demanded tunneling current, the number and positions of the barrier resonances can be controlled through the demanded tunneling current. In general, as the demanded tunneling current is reduced, the number of barrier resonances in the interval between -5 and -10 eV increases; however, the standing-wave spectrum takes a longer time to collect to achieve the same signal-to-noise ratio with the decreased signal amplitude. Here we use a constant demanded tunneling current of 1 nA, and compare data collected for different tips over a period of several months.

In Fig. 6(a) we show data collected with a tip that supports five barrier resonances over a $2\sqrt{3}$ domain. These resonances have been labeled $m=1$–5. Directly below this curve we show a spectrum collected with this same tip over a $\sqrt{3}$ domain. It can be seen that this spectrum has an additional peak at -7.5 eV, labeled with an arrow, between the $m=2$ and 3 barrier resonances of the $2\sqrt{3}$ spectrum. In addition, the higher-lying resonances in the $\sqrt{3}$ spectrum are phase shifted by 180°; the peaks in the $2\sqrt{3}$ spectrum are aligned with the troughs in the $\sqrt{3}$ spectrum beyond -7.5 eV.

In Fig. 6(b) we show data collected with a tip that supports six barrier resonances over a $2\sqrt{3}$ domain. Here the $m=3$ barrier resonance occurs at -7.5 eV and is thus degenerate with the structure at -7.5 eV associated with the thin-film resonance. The spectrum taken over the $\sqrt{3}$ domain appears to split the $m=3$ resonance into two peaks, and once again the higher-order barrier resonances are phase shifted by 180° between the two spectra.

In Fig. 6(c) we show data collected with a tip that supports seven barrier resonances over a $2\sqrt{3}$ domain. Now the extra peak in the spectrum taken over the $\sqrt{3}$ domain, labeled with an arrow, falls between the $m=3$ and 4 barrier resonances taken over the $2\sqrt{3}$ domain, and thus is no longer degenerate with these resonances. Again, the thin film creates an additional peak in the standing-wave spectra, and once again leads to a 180° phase shift between the two spectra for the higher-order barrier resonances.

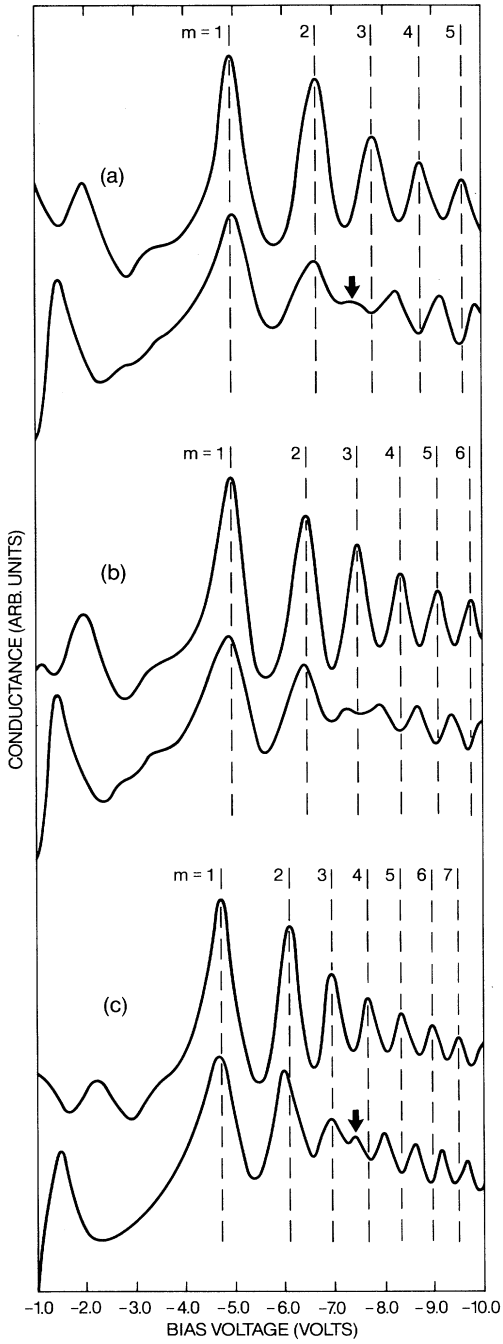

FIG. 6. Electron standing wave taken over $2\sqrt{3}$ and $\sqrt{3}$ domains using different tips. In (a) the spectra collected over the $2\sqrt{3}$ domain, top spectrum, had five conductance oscillations that have been labeled as $m=1,\ldots,5$. The corresponding spectra collected over a $\sqrt{3}$ domain using the same tip is shown in the lower spectrum. In (b) a different tip has six conductance oscillations over a $2\sqrt{3}$ domain, labeled $m=1,\ldots,6$ in the top spectrum. In (c) the tip supports seven standing-wave resonances over the $2\sqrt{3}$ domain, labeled $m=1,\ldots,7$ in the top spectrum. The thin-film resonance at -7.5 eV in the $\sqrt{3}$ domain spectra have been labeled with arrows in the spectra shown in (a) and (c). All spectra were collected with a demanded tunneling current of 1 nA.

V. DISCUSSION AND CONCLUSIONS

Standing-wave spectra collected over different domains of surface reconstructions, as shown in Figs. 4 and 5, display clear differences between the different domains. *This demonstrates that the geometry of the sample surface can have an influence on the formation of electron standing waves.* The defect-free $\sqrt{3}$ domain has been shown to support an extra density of states feature around -7.5 eV, which is absent over $2\sqrt{3}$ domains, over defects in the $\sqrt{3}$ domain, and over regions where there is intermixing of the overlayer and substrate atoms.

By collecting electron standing-wave spectra with tips that have different $S(V)$ characteristics, the coupling between the thin-film states and the vacuum barrier resonances can be examined. *In a sense, the barrier resonances can be "tuned" to have maxima at varying energies by using tips that follow different $S(V)$ trajectories.* This can be accomplished by varying properties of the tip such as its effective work function or sharpness. Lowering the work function of the tip, or decreasing the field necessary to draw the field-emission current through geometric field enhancement, leads to a broadening of the triangular potential well between the tip and sample, and thus a closer spacing of the well states. Alternatively, by varying the demanded tunneling current, the starting position for the tip above the surface as well as the field required to draw the demanded tunneling current can be varied, which has a similar effect on the energy position of the vacuum barrier resonance maxima.

When the thin-film resonance falls in energy between two vacuum barrier resonances, as in Figs. 6(a) and 6(c), the levels have a tendency to repel each other, with the greatest effect on the higher-order barrier resonances at energies above the thin-film resonance. The stronger barrier resonances below the thin-film resonance are pushed down only slightly, while the higher-order resonances are phase shifted 180°. When the thin-film resonance is degenerate in energy with a vacuum barrier resonance, as in Fig. 6(b), the level is split by the interaction, and the higher-order barrier resonances are once again repelled from the thin-film resonance, resulting in a 180° phase shift. These results are in agreement with the predictions of perturbation theory for coupled potential wells; the well levels are shifted when they are closely spaced in energy, and are split when they are degenerate.

Although there are strong interactions between these two different types of resonances, changing the spectrum of the resonances associated with the tip has been shown to have little or no effect on the resonance associated with the thin film; the thin-film resonance is the stronger of the two as it maintains its influence at -7.5 eV, splitting and repelling the resonances that form from reflections between the tip and sample. This also demonstrates the need for collecting standing-wave spectra under varying tip conditions when trying to determine the existence and energy of thin-film resonances. By "tuning" the position of the vacuum barrier resonances through the thin-film resonance, by using different tips or by varying the demanded tunneling current, the interactions between the two coupled wells can be determined.

So far the main practical application of the electron standing-wave technique for thin-film characterization has been for spatial imaging of buried interface inhomogeneities in epitaxial growth. Here, transitions between different overlayer orientations and thickness have been detected by the *spatial variation* of conductivity associated with these transitions in conductance maps[15,16] *at a given voltage.* With the ability to deconvolve thin-film resonances and vacuum barrier resonances in electron standing-wave spectra, by the techniques described here, the *energy spectrum* of the thin-film states can be determined *at a given spatial location,* thus providing additional information for determining the properties of thin-film overlayers.

ACKNOWLEDGMENTS

We thank R. S. Becker at AT&T Bell Laboratories for sharing the code used to render the STM images, and Tom Orlowski at Xerox for useful comments.

[1]G. Binnig and H. Rohrer, Helv. Phys. Acta. **55**, 726 (1982).
[2]R. S. Becker, J. A. Golovchenko, and B. S. Swartzentruber, Phys. Rev. Lett. **55**, 987 (1985).
[3]R. M. Feenstra, J. A. Stroscio, and A. P. Fein, Surf. Sci. **181**, 295 (1987).
[4]J. Bono and R. H. Good, Surf. Sci. **188**, 153 (1987).
[5]K. H. Gundlach, Solid-State Electron. **9**, 949 (1966).
[6]Y. R. Wang, J. A. Kubby, and W. J. Greene, Mod. Phys. Lett. B **5**, 1387 (1991).
[7]J. A. Kubby, Y. R. Wang, and W. J. Greene, Phys. Rev. Lett. **65**, 2165 (1990).
[8]R. H. Fowler and L. H. Nordheim, Proc. R. Soc. London Ser. A **119**, 173 (1928).
[9]J. G. Simmons, J. Appl. Phys. **34**, 1793 (1963).
[10]R. Young, J. Ward, and F. Scire, Phys. Rev. Lett. **27**, 922 (1971).
[11]T. Ando, A. B. Fowler, and F. Stern, Rev. Mod. Phys. **54**, 437 (1982).
[12]J. H. Coombs, M. E. Welland, and J. B. Pethica, Surf. Sci. **198**, L353 (1988).
[13]L. Scandella and H.-J. Guntherodt, Ultramicroscopy **42-44**, 546 (1992).
[14]J. M. Pitarke, F. Flores, and P. M. Echenique, Surf. Sci. **234**, 1 (1990).
[15]J. A. Kubby and W. J. Greene, Phys. Rev. Lett. **68**, 329 (1992).
[16]J. A. Kubby and W. J. Greene, J. Vac. Sci. Technol. B **10**, 1908 (1992).
[17]P. J. Estrup and J. Morrison, Surf. Sci. **2**, 465 (1964).
[18]T. Ichikawa, Surf. Sci. **140**, 37 (1984).
[19]J. Nogami, Sang-il Park, and C. F. Quate, J. Vac. Sci. Technol. A **7**, 1919 (1989).
[20]E. Ganz, I.-S. Hwang, F. Xiong, S. K. Theiss, and J. Golovchenko, Surf. Sci. **257**, 259 (1991).

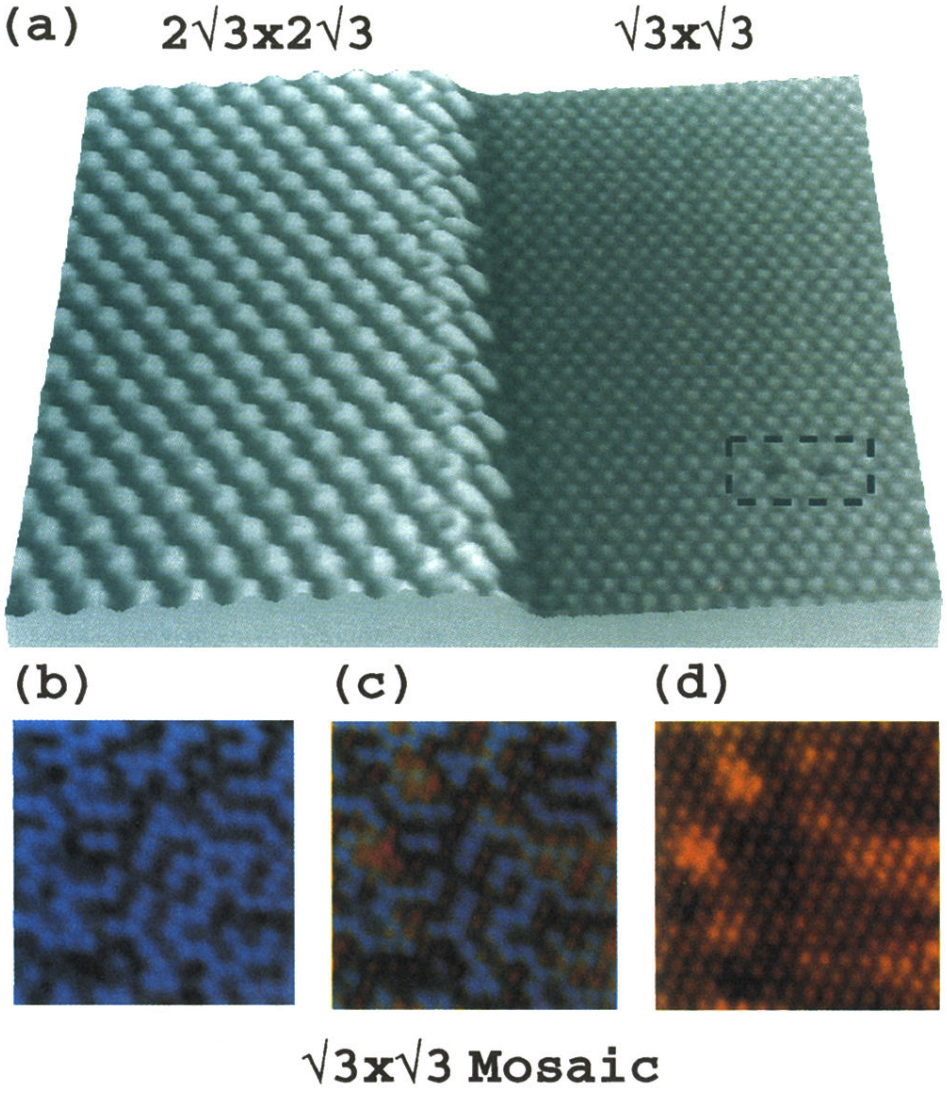

FIG. 4. Tunneling topographs of areas used for electron standing-wave excitation. (a) 250X 250-Å area containing $2\sqrt{3}$ reconstruction on the left and $\sqrt{3}$ reconstruction on the right. Some defects in the $\sqrt{3}$ domain have been outlined with a box. The image was collected at a tip bias of -1.5 V, tunneling into the sample empty states at a demanded tunneling current of 1 nA. (b) 100X100-Å domain of $\sqrt{3}$ mosaic, tunneling out of the samples filled states at a tip bias of $+1.0$ V, 1 nA. The corresponding empty-states image, collected simultaneously at -1.0 V, is shown in (d). The two are overlayed and the composite image is shown in (c).